Molecular Signal Tracking and Detection Methods in Fluid Dynamic Channels

Mahmoud Abbaszadeh, Iresha Atthanayake, Peter J. Thomas, and Weisi Guo, *Senior Member, IEEE*

Abstract—This method and data paper sets out the macro-scale experimental techniques to acquire fluid dynamic knowledge to inform molecular communication performance and design. Fluid dynamic experiments capture latent features that allow the receiver to detect coherent signal structures and infer transmitted parameters for optimal decoding. This paper reviews two powerful fluid dynamical measurement methodologies that can be applied beneficially in the context of molecular signal tracking and detection techniques. The two methods reviewed are Particle Image Velocimetry (PIV) and Planar Laser-Induced Fluorescence (PLIF). Step-by-step procedures for these techniques are outlined as well as comparative evaluation in terms of performance accuracy and practical complexity is offered. The relevant data is available on IEEE DataPort to help in better understanding of these methods.

Index Terms—molecular communication; experimentation; macro-scale; fluid dynamics; PIV; PLIF.

I. INTRODUCTION

Experimental molecular communications (MC) is critical for a number of research sectors, including: channel characterization [1]–[5], noise characterization for mutual information analysis [6]–[9], and system design (e.g. receiver size, mobility [8]). Experimental work is lacking at the macro-scale ($\geq$ 1mm), where molecular signals are subject to a variety of flow associated processes, most of which are dynamic and inter-related. Unlike the mass diffusion dominated regime (typically in micro-scale, 1μm-1mm, and nano scale, $\leq 1\mu$m), where the channel and noise model are well understood even for different modulation schemes [10]–[12], macro-scale continuum forces make analysis challenging. Macro-scale research is useful for a variety of underwater, gas/oil-pipe networks, chemical engineering, and electromagnetically denied applications.

Research at macro-scale requires significant undertaking and there is a growing body of work. Theoretical and simulation work on molecular communications with turbulence has shown that the fluid dynamic complexities cannot be ignored [2], [13]. Experimentation is essential to capture realistic variational behaviour in fluid dynamics. It can enable us to 1) find stable coherent structures in fluids that point towards better

modulation design (e.g., generated self-propagating structures to increase symbol rate and transmission range [14]), and 2) infer channel parameters to aid receiver signal decoding (e.g. maximum likelihood estimation [15]).

An overview of experimental molecular communications is given in [16]. Early prototyping experimental work started with tabletop prototypes characterizing experimental throughput [17]–[22] and noise processes [23] with crude chemical sensors, which has now advanced to encoding in chemical mixtures [24], [25] with mass spectrometer demodulation. This coincides with parallel work in replicating pheromone signals [26]. In our attempts to understand and improve the achievable mutual information in macro-scale fluid dynamic channels with complex processes, recent work (2017-19) has characterized the evolving information structure in turbulence [3] and tracked info-molecules using fluorescence [4], [27], [28].

A. Key Metrics for Signal Measurement

In all the aforementioned work in macro-scale experimental MC, measuring key attributes of molecular signals are essential. The key attributes are closely related to the manner in which information is modulated to the molecular signal [1]. In concentration-shift-keying (CSK), measuring the concentration of the flow field is important. In pulse-position-modulation (PPM) measuring the time of arrival difference between sequential pulses is important. We can generally either measure the concentration directly, or measure the flow attributes to extract or infer the concentration, as well as other flow attributes. It is worth mentioning that other chemical modulation schemes that encode information in chemical structure (e.g. molecular shift keying) and ratio of chemical mixtures in compounds (e.g. isomer-based shift keying and pheromones), require a mass spectrometer [24] or proprietary electronic nose [26].

In laminar flow, measured concentration or flow attributes can be directly related to laminar flow parameters (e.g. flow speed increases signal-to-noise ratio and throughput [4]). However, in turbulent flow, additional processes must be taken into account in terms of the turbulence structure and the size of the eddies. The terms eddy and vortex are used to describe the swirling motion of a fluid. The word eddy is usually associated with small-scale swirling entities whereas a vortex, such as a large-scale tornado, contains eddies on smaller spatial scales. Eddies are created, for instance, when a fluid is injected from a syringe into another larger fluid volume due to the momentum difference and shear stress at the fluid interface. If the injected momentum is high enough mixing leads to a turbulent patch

M. Abbaszadeh and P. J. Thomas are with the School of Engineering, University of Warwick, Coventry CV4 7AL, U.K, (e-mail: m.abbaszadeh@warwick.ac.uk; p.j.thomas@warwick.ac.uk)

I. U. Atthanayake is with the Mechanical Engineering Department, Open University, Sri Lanka (e-mail: ireshairesha@yahoo.com).

Weisi Guo is with the University of Warwick, Coventry CV4 7AL, U.K., also with The Alan Turing Institute, London NW1 2DB, U.K., and also with the School of Aerospace, Transport and Manufacturing, Cranfield University, Bedford MK43 0AL, U.K. (e-mail: weisi.guo@cranfeild.ac.uk).

comprising eddies of different diameters. The diameter of an eddy is its characteristic length scale. By analyzing the size distribution of eddies within a turbulent flow one can extract information about the features of turbulence. As the turbulent patch evolves in time there exists a cascade involving larger eddies breaking up in to smaller ones. This evolving process leads to transport of energy from larger to smaller scales, referred to as the **energy cascade**, until the energy is dissipated at a critical length scale by the action of viscosity. This smallest scale is known as the Taylor microscale. At this scale fluid viscosity significantly affects the dynamics of the turbulent eddies in the flow (see e.g. [29]). Small eddies, near the Taylor microscale where viscous effects dominate, do not contribute significantly to the transport of information. This is considered as the lower bound for the molecular communication capacity [3].

B. Novelty and Organization of Paper

Particle Image Velocimetry (PIV) and Planar Laser-Induced Fluorescence (PLIF) are standard measurement techniques in fluid dynamics [30], [31]. However, to the best of our knowledge, this is the first MC paper to detail PIV and PLIF methods for measuring flow field and concentration properties. The protocol to apply these experimental methods and how to post-process the acquired data are described in detail in this paper.

This method and data paper builds on the authors' own work over the past 3 years funded by United States Air Force Office for Scientific Research (US AFOSR), Defence Science Technology Laboratory (DSTL), and EC H2020. We have developed macro-scale experimental capability that can faithfully track molecular information to translate fluid-dynamic knowledge in the context of MC.

We used our setup in Ref. [4], [9] to measure the information rate in turbulent and laminar channel flows and to characterize the noise model in these channels. In particular, the setup in [4] uses the PIV method, whereas the PLIF method is applied in [9]. Here, we discuss more general aspects of the equipment and of the experimental procedures such that corresponding studies can be reproduced more easily and reliably elsewhere.

The paper is organized as follows: the experimental setup is described in Section II. In Section III the PIV method for the measurement of flow velocities is outlined together with a brief discussion of alternative techniques. Correspondingly Section IV introduces the PLIF method, and alternatives, for the measurement of the concentration of fluorescent tracers transported along with the flow. Section V and Section VI contain, respectively, the discussion and the conclusion.

II. EXPERIMENTAL SET UP

A. Armfield Flume (Channel)

The Armfield flume (channel) used for our studies is shown in Fig.1(a). The open channel is $15\,\mathrm{m}$ long, $0.3\,\mathrm{m}$ wide, and $0.6\,\mathrm{m}$ deep. The channel has glass side walls providing convenient optical access. The flow rate of the channel is controlled by means of a pump. This enables setting the mean flow velocity to a desired constant value. To maintain a constant water level within the flume an inclined plate is mounted at the channel outlet. The recirculating liquid has to spill across this plate. By adjusting the angle of the plate one can therefore set the water level inside the flume.

The injection system comprises a syringe-pump arrangement illustrated in Fig. 1(b). The syringe pump is driven by a computer-controlled stepper motor and enables ejecting precisely defined volumes of fluorescent tracer liquid into the flow field. The electronic components required to drive the stepper motor, which is controlled by an Arduino program, are contained in a small box.

The transmitter for the release of fluorescent tracer liquid is displayed in Fig. 1(c). It constitutes a bent pipe with a diameter of $5\,\mathrm{mm}$. The inlet of the pipe is connected to the solenoid valve and the outlet is located submersed under water inside the channel. The transmitter is mounted such that its position within the channel can be varied.

Fig. 1(d) displays the components forming the receiver of our experimental set-up. The receiver comprises a laser to generate a light sheet for the illumination of a cross section of the flow and a video camera as a means for recording the experiments for the subsequent data analysis using the relevant methods. The purpose of these two individual receiver components within the arrangement are discussed in detail in Sections III and IV.

B. Reynolds Number

A Reynolds number is defined to characterize the overall flow conditions within the channel. The physical meaning of the Reynolds number is that it represents the approximate ratio of inertial forces and viscous forces in the flow. For open-channel flow the Reynolds number is defined as [32]:

$$Re = \frac{u \times L}{\nu} \, , \tag{1}$$

where u is the mean flow velocity and ν is the kinematic viscosity of the liquid. The quantity L represents the characteristic length scale for open channel flow. It is equal to the hydraulic radius of the channel given by A/p, where A is the cross-sectional area of the flow and p is the wetted perimeter of the channel [32]. For open channels the flow remains laminar for, approximately, $Re < 500$ and it transitions to turbulent flow above this critical value [32]. In our experiment, $\nu = 10^{-6}\,\mathrm{m}^2\mathrm{s}^{-1}$, $u = 0.2\,\mathrm{ms}^{-1}$, and the Re=16000.

III. PARTICLE IMAGE VELOCIMETRY (PIV)

The most frequently used modern technique for the analysis of flow fields is PIV. PIV is an optical technique used for the measurement of flow velocities and it thereby provides a tool for flow visualization. The method is referred to as non-intrusive since it is not required to insert flow sensors in the flow field that can potentially alter aspects of the dynamics to be monitored. Technical details of the methodology are
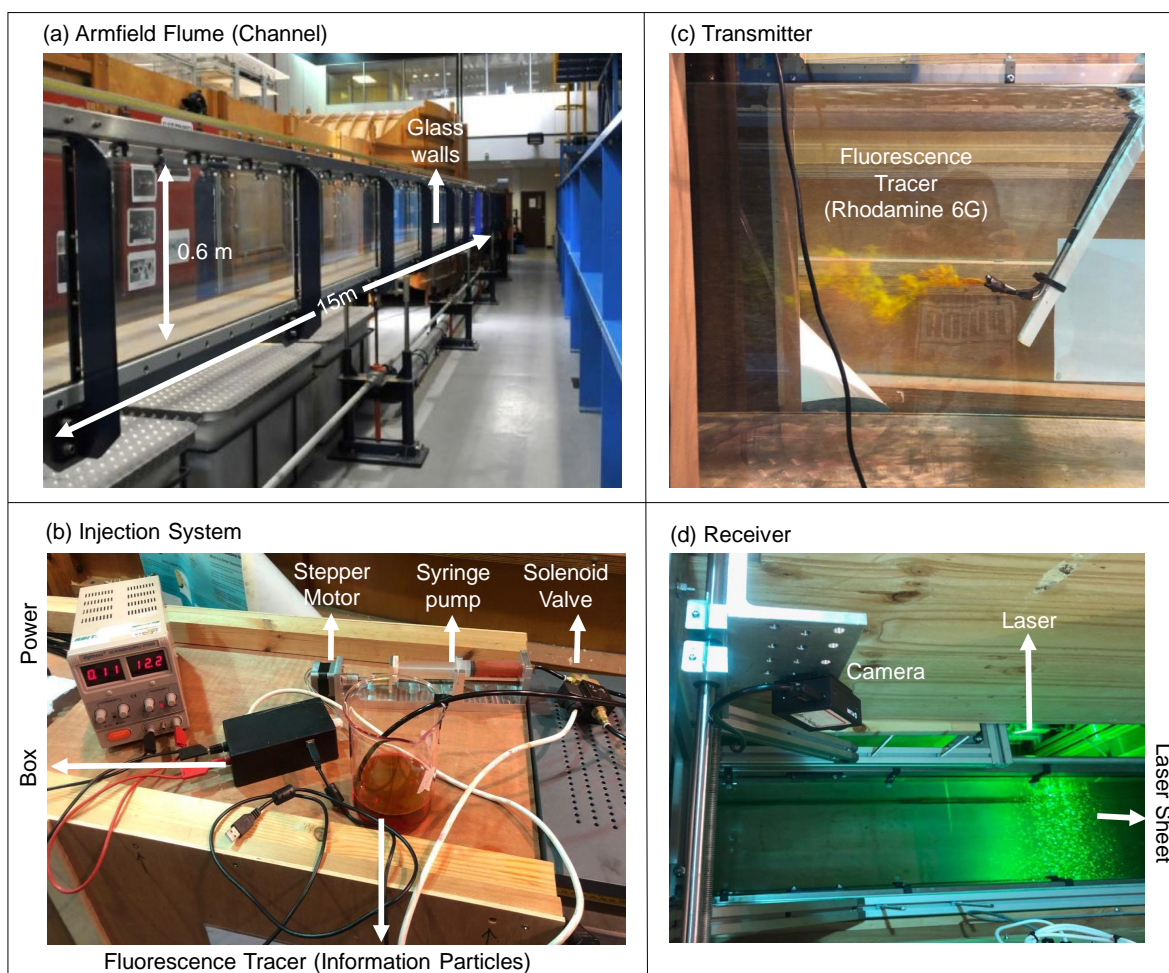
Fig. 1: a) Armfield-flume (channel) configuration. It is $15\,\mathrm{m}$ long, $0.3\,\mathrm{m}$ wide, and $0.6\,\mathrm{m}$ deep, b) Injection system including power, electronic boards and the syringe pump, c) Transmitter pipe, d) Receiver station.

summarized in [30]. The following steps are required for a typical PIV measurement.

- **Tracer:** The flow is seeded with micron-sized tracer particles. Ideally seeding particles are chosen that are neutrally buoyant. This is required such that the particles always faithfully follow the flow and therefore accurately represent the flow velocity at their locations within the flow field [33]. In liquids one can use, for instance, hollow-glass spheres as seeding particles, which can be silver-coated to increase their reflectivity as is the case in the experiments of [4], [34]. If the flow is in a gas, then it is not possible to satisfy the requirement for neutral buoyancy and one typically uses, for instance, micron-sized oil droplets as tracer particles.
- **Imaging:** A laser and an optical arrangement, comprising a cylindrical lens, is used to generate a thin light sheet that intersects the flow as illustrated in Fig. 2 (see Table I). Tracer particles moving within the light sheet become brightly illuminated. Thus, their motion can be recorded by means of a video camera.
- **Analysis:** On any two successive video images taken

at a short time interval $\Delta t = t' - t$ apart the tracer particles will appear at slightly shifted locations due to their motion while following the flow field (see Fig. 2). By analyzing from where to where particles have moved within the image plane in the known time interval Δt, it is possible to infer the magnitude and the direction of the particle velocity and the flow velocity. Once the basic velocity field is known as a function of time, other quantities such as time averaged velocities, the vorticity or the turbulence characteristics can be obtained from post-processing of the collected data. An in-depth example showing such results from a PIV study is discussed in [34].

A. Processing PIV images

1) Image processing: In order to process the PIV data, the raw images (Fig. 3(a1)) taken in successive frames are uploaded to the PIVlab software [35]. The Matlab based PIVlab software is an open-source tool for the analysis and post processing of PIV data. The full tutorial and MATLAB application of PIVlab are at (https://pivlab.blogspot.com). The

TABLE I: Summary of features of PIV and PLIF methods. Equipment needed for running experiment and websites for purchasing those equipment.

|	Particle Image Velocimetry (PIV)	Planar Laser-Induced Fluorescence (PLIF)
Features	- Non-intrusive - Currently normally gives velocity in 2D plane but and 3D methods are now becoming available - Low resolution - Hazardous (laser) - Requires transparent liquid	- Non-intrusive - Yields concentration distribution in a 2D plane - Hazardous (laser) - Requires transparent liquids
Equipment	- Laser (Pulsed frequency doubled Nd: YAG at 532 nm wavelength) - Cylindrical lens - Camera (High-speed CMOS camera) - Seeding particles (Hollow glass spheres, Polystyrene, Oxygen bubbles) - External hard drives	- Laser (Pulsed frequency doubled Nd: YAG at 532 nm wavelength) - Camera (High-speed CMOS camera) - Notch filter for the camera (OD 6.0) - Seeding particles (Rhodamine 6G) - External hard drive
Website	Dantecdynamics.com; TSI.com; Lavision.de; Oxfordlasers.com	Dantecdynamics.com; TSI.com; Lavision.de; Oxfordlasers.com
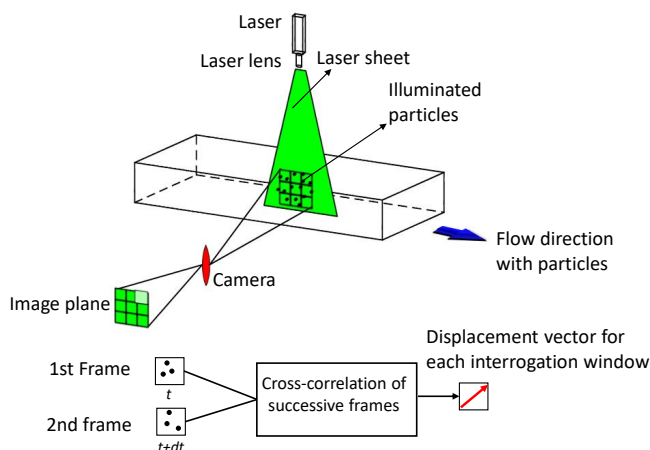
Fig. 2: Schematic of PIV set-up. A Laser sheet illuminates a plane section of the flow. The flowing liquid contains small tracer particles following the flow and therefore representing the flow velocity. The particles are illuminated brightly by the laser light when travelling within the light sheet. The camera captures the motion of the tracer particles in successive frames. Cross-correlation of successive images yields the velocity field.

principles of PIV which are briefly summarized by means of Fig. 3(a2) shows an image taken from a flow field. The camera is focused on the area in the centre of the image, the area of interest. Here the particles are in focus whereas they are somewhat blurred towards the edge of the image frame. Only the area of interest is considered for further analysis of the flow field. To this end, the video images are divided into small **interrogation regions** and corresponding interrogation regions in successive video frames are compared. Figure 3(a3) displays a PIV image that is divided into interrogation areas of 15×20 pixels. A pair of two consecutive instantaneous video images which are separated by time $\Delta t = 0.01$ s is shown in Fig. 3(b). Each interrogation area of the second image, taken at time $t + \Delta t$, is shifted relative to the first image taken at t. A cross correlation between the two images

is performed (see the MATLAB code and velocity vector in Fig. 3(b)). That particular shift for which the correlation function adopts its maximum is then taken as the direction in which the particles within the small interrogation region have collectively travelled. This direction together with the time interval Δt between the two video frames then defines the magnitude and the direction of the flow velocity at the location of the interrogation region [36].

2) Calibration: The PIV methodology requires calibration to provide a conversion factor relating distances in terms of pixels to their corresponding real-world distance in units of length. For the calibration process a calibration image is used. Figure 3(c1) displays a typical calibration image which, in this particular case, consists of rows of black circles of constant radius on a white background. The radius of the circles and the distance between their centres represent known reference lengths. Once the real distance of particle displacement is known, a velocity vector for the considered interrogation area is determined. A velocity-vector map over the whole image area is obtained by repeating the procedure outlined in Section III-A-1 for each interrogation area over the entire image. Figure 3(c2) shows a typical velocity-vector field calculated from a PIV image pair.

B. PIV in Comparison to Other Methods

There are alternative methods for velocity monitoring. One other popular optical technique is Laser Doppler Anemometry (LDA), frequently referred to as Laser Doppler Velocimetry (LDV) [37]. Similar to PIV the LDV technique is a non-intrusive methodology that requires optical access to the flow field but no sensors within the flow field. Other common non-optical methods are Hot-Wire Anemometry (HWA) [38], [39], and Ultrasonic Velocity Profilers (UVP) [40].

However, for most applications the PIV technique has advantages over all the other methods since it gives the 2D flow field and it is also non-intrusive. Note that with more sophisticated technical arrangements 3D flow field monitoring by means of PIV is nowadays increasingly becoming a viable option.
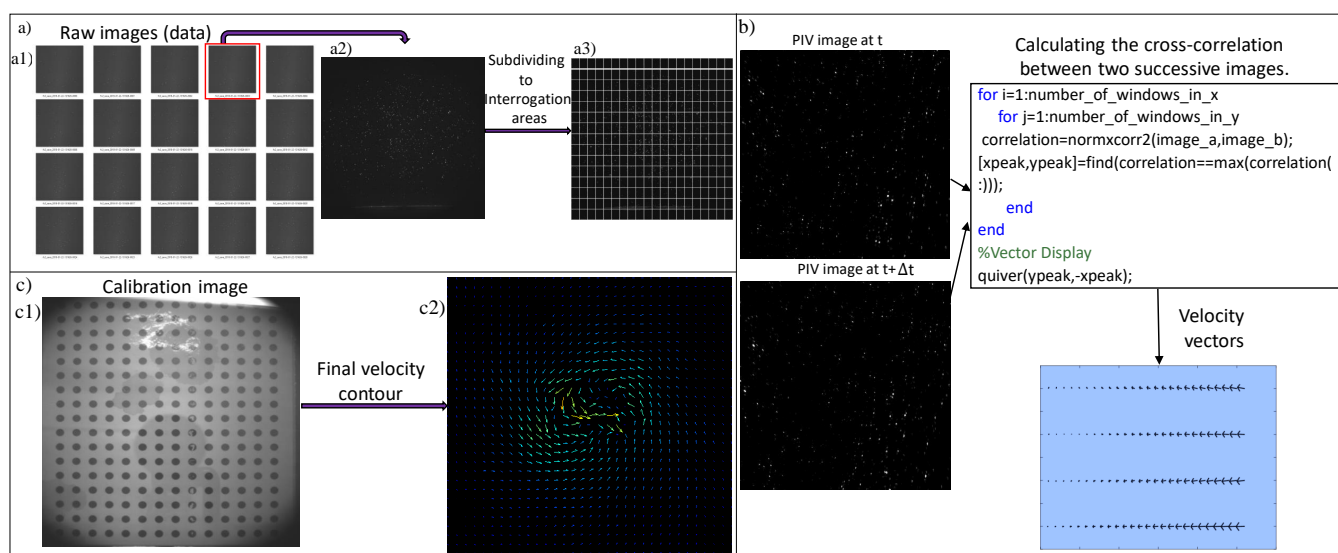
Fig. 3: a) First stage in PIV image processing, a1) Raw PIV images, a2) An original PIV image in the vertical plane, a3) PIV image with sub divided interrogation areas; b) Two PIV images taken at times t and t+Δt: Δt = 0.01 s, cross correlation MATLAB code and velocity vectors obtained by calculating cross correlation; c) Final stage of converting pixel distance to read distance, c1) The calibration plate in the vertical plane, c2) Velocity vector field obtained by analysing a PIV image pair.

Similar to PIV, the LDA and UVP techniques also rely on inferring velocity data from the motion of tracer particles carried along with the flowing medium. While PIV relies on monitoring the tracer- particle displacement in the image plane the LDA and the UVP methodology infer the velocity of the tracer particles from the Doppler shift of the scattered and detected laser light (LDA) and the ultrasound waves (UVP).

A distinguishing feature of UVP is that, unlike light, ultrasound can propagate through transparent and opaque materials. This means that the probe emitting the ultrasound for the UVP method can be mounted inside the flow field or outside of the material walls enclosing the flow. Thus, UVP can be operated in intrusive or in non-intrusive mode. Most importantly, however, the UVP methodology also enables measuring flow velocities within opaque liquids, such as liquid metals.

While the type of PIV system in Fig. 2 yields data for the whole light sheet plane, an LDA system only allows the velocity to be monitored at a single location. In comparison to LDA, the UVP technology is more versatile in that it yields velocity data not only at a single location but for a section near the probe on the straight trajectory along which the transmitted ultrasound beam propagates through the flowing liquid.

Hot-wire anemometry (HWA) is an intrusive technology and requires a small, very fragile and expensive, measurement probe to be inserted into the flow field [41]. Similar to the LDA method HWA can only measure the velocity at a single location. A HWA probe with a single wire is uni-directional and can only detect one flow component. However, there exist probes with two or three wires to measure more than one velocity component.

IV. PLANAR LASER INDUCED FLUORESCENCE (PLIF)

Planar laser induced fluorescence is an optical diagnostics technique that can measure the concentration of a fluorescent tracer dye as it gets carried along and diluted in a fluid flow [31].

Similar to PIV, PLIF technique requires a cross-section of the flow to be intersected by a laser light sheet as illustrated in Fig. 4. After a tracer fluorescence (or information particle) is injected, it is carried along by the fluid flow towards the laser sheet. The laser light excites fluorescence and images are captured to record the intensity of the shining fluorescence. The fluorescence intensity is primarily dependent on the tracer concentration and is used as a parameter to show the concentration of the tracer. A tracer frequently used is Rhodamine 6G; this has peak adsorption at a wavelength of 532 nm and peak emission at around 560 nm [42].

In typical signal-transmission experiments a known amount of liquid, containing a certain concentration of the fluorescent tracer, can be released from, for instance, a small nozzle within the flow field. The fluorescent liquid is then viewed as representing information carrying particles released by a sender. Thus, the fluorescence pattern that becomes visible within the light sheet provides a visual representation of the dynamic behaviour of the information-carrying liquid particles as they get carried along in the flow and, facilitated by the action of eddies and turbulent flow fluctuations, mix with ambient liquid.

PLIF can be combined with PIV to concurrently obtain concentration and velocity data. Table I on page 4 summarizes the main features of PIV and PLIF together with the required equipment and websites of commercial product suppliers.
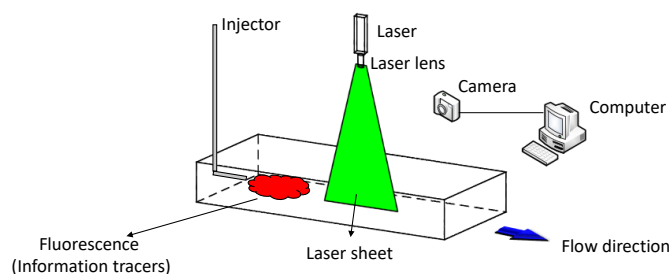
Fig. 4: Schematic of PLIF. Laser sheet excites the fluorescence injected by the transmitter and the camera captures the intensity of excited fluorescence.

A. PLIF Imaging Equipment

The radiant power of the laser is 1000 mW. The working voltage of the laser is 110-220 VDC and the working current of the laser is less than $1500\,\text{mA}$. The beam diameter of the laser is $1\,\text{mm}$ with the wavelength of $532\,\text{nm}$ green color. The laser beam passes through a cylindrical lens to generate a laser sheet. The power intensity of the laser sheet has a Gaussian profile. A notch filter is positioned in front of the camera to remove light not required for the data analysis. In the case of Rhodamine 6G, for instance, light below $550\,\text{nm}$ should be filtered out such that only the light from the emission peak at $560\,\text{nm}$ is detected by the camera. A high-speed CMOS camera captures the light emanating from the Rhodamine 6G tracer illuminated within the laser sheet. The viewing direction of the camera is required to be perpendicular to the light sheet to avoid any parallax data bias. The model and properties of the camera and laser used in the PLIF are included in Table I on page 4.

Figure 5(a) shows images captured at different times at the receiver. The average image intensity for each image was calculated in MATLAB and it is displayed in Fig. 5(a) as a function of time t. It is now required to associate the average image intensity with a corresponding dye concentration to yield a calibration curve.

B. Calibration

The relation between the mean image intensity and the dye concentration can be determined by first preparing and then video recording water-dye solutions of known concentration at the location of the receiver. The one-to-one calibration mapping between the Rhodamine 6G concentration and the mean intensity for our experiments is shown in Fig. 5(b). Note that the calibration curve increases linearly for the dye concentrations used. However, for very high concentrations the linear behaviour will break down and asymptotically converge to a saturation value. The final graph displaying the concentration as a function of time is displayed in Fig. 5(d).

C. PLIF in comparison to the sensors

An alternative method for measuring the concentration of tracers contained in a liquid is provided by a variety of active electronic (e.g. electronic nose) and passive optical

sensors. Using sensors is straightforward and has the advantage of not requiring a laser. However, the disadvantage of sensors in comparison to laser-based methods is that they are intrusive and have to be submersed in the flow field. One commonly used sensor is the Turner Designs CYCLOPS-7 Submersible Fluorometer [43]. Rhodamine WT, where WT stands for "water tracing", is often used as the fluorescent tracer but there are others. The sensor displays and records the level of the tracer concentration in terms of an output voltage. The output voltage increases linearly with the concentration level in the measurable range of the fluorometer.

V. DISCUSSIONS

A. Data-set

Sample images of PIV and PLIF experiments have been uploaded to the IEEE Dataport, DOI: 10.21227/eae4-kg81. They are in 22 zip files, the first two files are for the PIV measurement and the others are for the PLIF experiment. PIV test files contain 654 and 1392 images for frame rates of 15 and 90 fps, respectively. The image format is .bmp, and the first image in each set is the calibration image. There are 20 zip files named PLIF-1 to PLIF-20. Each file contains approximately 150 images in TIF format. The first 25 images in each file are calibration images and the rest are images of the laser plane after injection of the tracer fluorescence. All images are recorded with a frame rate of 2 fps so one can calculate the total recording time according to the number of images per file. The MATLAB code has also been provided for each file and assists with the required image processing.

B. Experimental Data Aids Communication Understanding

Noise characterization is important for understanding the achievable mutual information in these complex signaling environments [6]–[8]. Analytical noise expressions from mass diffusion channels for concentration modulation [44], [45] and timing modulation [10], [11], [46] are well understood. By modeling the noise empirically using our reviewed experimental techniques, one is able to calculate the mutual information either analytically for Gaussian distributed noise [4], [8], or numerically via non-Gaussian distributed noise [47]. Extracting both the additive and jitter noise distribution can be conducted and further analysis of the mutual information can be conducted to understand the optimal transmission strategy to maximize the mutual information. Our technical paper in [9] details how these methods are applied in characterizing the noise model in a turbulent channel. As the first example, here we show how to characterise the noise using the PLIF images. Each PLIF file in the data-set displays one channel impulse response (CIR). All 20 CIRs have been performed under the same initial conditions. One should plot all 20 CIRs together to calculate the additive and jitter noise, respectively by fitting a probability distribution to the peak concentration values and the values of time that peak concentration occurs.

After characterising the noise for the channel it is required to define the channel model for macro-scale MC. The channel
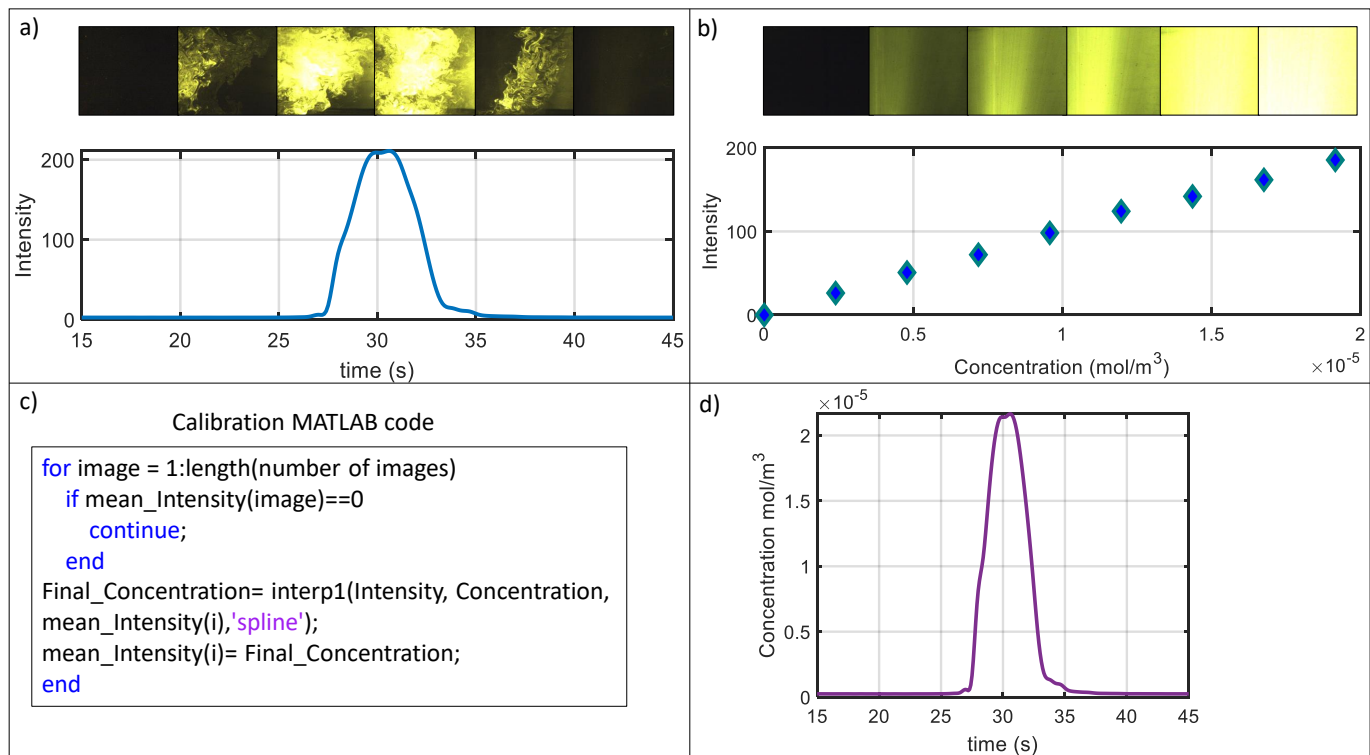
Fig. 5: Step-by-step post processing of PLIF method. a) Intensity of the images in terms of time at the receiver, b) Calibration curve obtained from the calibration images, c) Calibration MATLAB code for mapping between intensity and concentration, d) Final Concentration versus time after calibrating.

model that is widely used in macro-scale scale MC is derived by solving the advection-diffusion equation:

$$\frac{\partial c}{\partial t} = \nabla \cdot (D_\varepsilon \nabla c) - \nabla \cdot (\vec{v}c), \qquad (2)$$

where c is the concentration and D_ε is the eddy diffusivity coefficient. The amount of molecules released into the channel at $t = 0$ is identified by c_0 and v is the flow velocity. The variation of the velocity with space and time is required for solving (2). As the second example, here we show that how the PIV images should be used to calculate the velocity field. One should calculate the ensemble average of the velocity in each interrogation area (see Fig. 3(a3)) to obtain the velocity field. After calculating the velocity, it should be substituted into (2) to obtain the concentration and channel model.

C. Experimental Recommended Practice

PIV and PLIF methodologies involve lasers and they require compliance with the relevant health and safety regulations. Lasers have potential hazards to the human eye and skin from both direct and scattered beam exposure. The radiant power of lasers used in PIV generally have around $1000\,\mathrm{mW}$ with a wavelength of $532\,\mathrm{nm}$ and a beam diameter of $1\,\mathrm{mm}$ (for optimal water transmission). To understand safety, we calculate the maximum permissible exposure (MPE), which is the highest power or energy density of a light source that is considered safe. It is usually about 10% of the dose that has a 50% chance of creating damage under worst-case conditions.

The MPE is measured at the cornea of the human eye or at the skin, for a given wavelength and exposure time. Our beam divergence is 3 milli-radians (0.003 radians) and $25\,\mathrm{W\,m^{-2}}$ is the eye MPE for a single accidental exposure to a continuous wave (CW) laser beam from 400 to $700\,\mathrm{nm}$. The laser delivery system produces a beam plane which is $0.3\,\mathrm{m}$ wide, aligned perpendicular to the long axis of the fluid channel. To counter this, the laser area must be fitted into an enclosure to cover the Nominal Ocular Hazard Distance (NOHD) [48]:

$$\mathrm{NOHD} = \frac{\sqrt{\frac{4 \times \mathrm{radiant\ power}}{\pi \times \mathrm{MPE}}} - \mathrm{initial\ beam\ diameter}}{\mathrm{beam\ divergence}}, \qquad (3)$$

which is the distance from the source at which the intensity or the energy per surface unit becomes lower than the MPE on the cornea and on the skin. In our setup, the NOHD is 3.5 m.

VI. CONCLUSIONS

The PIV and PLIF methodologies for tracking and detection of molecular signals were reviewed. The focus was on the individual steps required to perform measurements with both techniques and on the data, relevant to molecular communication, that can be obtained by the methodologies. Fluid dynamic experiments in molecular communication generally aim to measure 1) flow parameters that are proxy for the channel parameters to aid receiver side signal processing (e.g. maximum likelihood detection), and 2)

coherent structures (e.g. vortex rings) that are a proxy for modulating information. Finally, the key message is that often both methods are required to capture both the key molecular signal information (e.g. concentration measurement) while concurrently tracking the channel parameters that caused it (e.g. flow measurement).

REFERENCES

[1] W. Guo, T. Asyhari, N. Farsad, H. B. Yilmaz, B. Li, A. Eckford, and C.-B. Chae, "Molecular communications: channel model and physical layer techniques," *IEEE Wireless Communications*, vol. 23, no. 4, pp. 120–127, August 2016.

[2] B. D. Unluturk and I. F. Akyildiz, "An end-to-end model of plant pheromone channel for long range molecular communication," *IEEE Transactions on Nanobioscience*, vol. 16, no. 1, pp. 11–20, 2017.

[3] E. Kennedy, P. Shakya, M. Ozmen, C. Rose, and J. Rosenstein, "Spatiotemporal information preservation in turbulent vapor plumes," *Applied Physics Letters*, vol. 112, pp. 666–697, 2018.

[4] I. Atthanayake, S. Esfahani, P. Denissenko, I. Guymer, P. J. Thomas, and W. Guo, "Experimental molecular communications in obstacle rich fluids," *Proc. ACM Int. Conf. on Nanoscale Comput. Commun. (NANOCOM)*, 2018.

[5] L. Khaloopour, S. V. Rouzegar, A. Azizi, A. Hosseinian, M. Farahnak-Ghazani, N. Bagheri, M. Mirmohseni, H. Arjmandi, R. Mosayebi, and M. Nasiri-Kenari, "An experimental platform for macro-scale fluidic medium molecular communication," *IEEE Transactions on Molecular, Biological and Multi-Scale Communications*, 2020.

[6] M. J. Moore, T. Suda, and K. Oiwa, "Molecular communication: Modeling noise effects on information rate," *IEEE Transactions on NanoBioscience*, vol. 8, no. 2, pp. 169–180, June 2009.

[7] M. Pierobon and I. F. Akyildiz, "Capacity of a diffusion-based molecular communication system with channel memory and molecular noise," *IEEE Transactions on Information Theory*, vol. 59, no. 2, pp. 942–954, Feb 2013.

[8] L. Lin, Q. Wu, F. Liu, and H. Yan, "Mutual information and maximum achievable rate for mobile molecular communication systems," *IEEE Transactions on NanoBioscience*, vol. 17, no. 4, pp. 507–517, Oct 2018.

[9] M. Abbaszadeh, W. Li, L. Lin, I. White, P. Denissenko, P. J. Thomas, and W. Guo, "Mutual information and noise distributions of molecular signals using laser induced fluorescence," in *2019 IEEE Global Communications Conference (GLOBECOM)*, 2019, pp. 1–6.

[10] W. Haselmayr, N. Varshney, A. T. Asyhari, A. Springer, and W. Guo, "On the impact of transposition errors in diffusion-based channels," *IEEE Transactions on Communications*, vol. 67, no. 1, pp. 364–374, 2019.

[11] A. Etemadi, P. Azmi, H. Arjmandi, and N. Mokari, "Compound poisson noise sources in diffusion-based molecular communication," *IEEE Transactions on Communications*, pp. 1–1, 2019.

[12] A. Noel, K. C. Cheung, and R. Schober, "A unifying model for external noise sources and ISI in diffusive molecular communication," *IEEE Journal on Selected Areas in Communications*, vol. 32, no. 12, pp. 2330–2343, Dec 2014.

[13] M. Abbaszadeh, H. B. Yilmaz, P. J. Thomas, and W. Guo, "Linearity of sequential molecular signals in turbulent diffusion channels," in *ICC 2019 - 2019 IEEE International Conference on Communications (ICC)*, May 2019, pp. 1–6.

[14] M. Abbaszadeh, P. J. Thomas, and W. Guo, "Towards high capacity molecular communications using sequential vortex rings," *IEEE Transactions on Molecular, Biological and Multi-Scale Communications*, 2018.

[15] L. Meng, P. Yeh, K. Chen, and I. F. Akyildiz, "On receiver design for diffusion-based molecular communication," *IEEE Transactions on Signal Processing*, vol. 62, no. 22, pp. 6032–6044, 2014.

[16] W. Haselmayr, A. Springer, G. Fischer, C. Alexiou, H. Boche, P. Hoeher, F. Dressler, and R. Schober, "Integration of molecular communications into future generation wireless networks," *Proceedings of 1st 6G Wireless Summit*, 2019.

[17] N. Farsad, W. Guo, and A. W. Eckford, "Tabletop molecular communication: Text messages through chemical signals," *PloS one*, vol. 8, no. 12, p. e82935, 2013.

[18] B. Koo, C. Lee, H. B. Yilmaz, N. Farsad, A. Eckford, and C. Chae, "Molecular mimo: From theory to prototype," *IEEE Journal on Selected Areas in Communications*, vol. 34, no. 3, pp. 600–614, March 2016.

[19] P. N. Prasanth, K. P. Sumanth, V. K. Chakka, and G. Roy, "Experimental implementation of molecular communication system using sampling based adaptive threshold variation demodulation algorithm," in *2018 IEEE International Conference on Advanced Networks and Telecommunications Systems (ANTS)*. IEEE, 2018, pp. 1–5.

[20] Song Qiu, W. Guo, S. Wang, N. Farsad, and A. Eckford, "A molecular communication link for monitoring in confined environments," in *2014 IEEE International Conference on Communications Workshops (ICC)*, June 2014, pp. 718–723.

[21] P. Lu, Y. You, B. Liu, and Z. Wu, "A vertical channel model of molecular communication based on alcohol molecules," *ACM Int. Conf. on Bio-inspired Information and Communications Technologies (BICT)*, pp. 157–162, 2016.

[22] H. Unterweger, J. Kirchner, W. Wicke, A. Ahmadzadeh, D. Ahmed, V. Jamali, C. Alexiou, G. Fischer, and R. Schober, "Experimental molecular communication testbed based on magnetic nanoparticles in duct flow," in *2018 IEEE 19th International Workshop on Signal Processing Advances in Wireless Communications (SPAWC)*, June 2018, pp. 1–5.

[23] N. Farsad, N. Kim, A. W. Eckford, and C. Chae, "Channel and noise models for nonlinear molecular communication systems," *IEEE Journal on Selected Areas in Communications*, vol. 32, no. 12, pp. 2392–2401, Dec 2014.

[24] D. T. McGuiness, S. Giannoukos, A. Marshall, and S. Taylor, "Experimental results on the open-air transmission of macro-molecular communication using membrane inlet mass spectrometry," *IEEE Communications Letters*, vol. 22, no. 12, pp. 2567–2570, Dec 2018.

[25] D. T. McGuiness, S. Giannoukos, S. Taylor, and A. Marshall, "Experimental and analytical analysis of macro-scale molecular communications within closed boundaries," *IEEE Transactions on Molecular, Biological and Multi-Scale Communications*, 2019.

[26] M. Cole, J. W. Gardner, Z. Ráczu, S. Pathak, T. C. Pearce, J. Challiss, D. Markovic, A. Guerrero, L. Muñoz, G. Carot, B. S. Hansson, S. Olsson, L. Kübler, J. G. E. Gardeniers, N. Dimov, and W. Bula, "Biomimetic insect infochemical communication system," in *IEEE Sensors*, Oct 2009, pp. 1358–1361.

[27] N. Tuccitto, G. Li-Destri, G. Messinaa, and G. Marlettaa, "Fluorescent Quantum Dots Make Feasible Long-Range Transmission of Molecular Bits," *ACS Physical Chemistry Letters*, 2017.

[28] M. Ozmen, E. Kennedy, J. Rose, P. Shakya, J. K. Rosenstein, and C. Rose, "High speed chemical vapor communication using photoionization detectors," in *IEEE Global Communications Conference (GLOBECOM)*, Dec 2018, pp. 1–6.

[29] P. A. Davidson, *Turbulence: an introduction for scientists and engineers*. Oxford University Press, 2015.

[30] M. Raffel, C. E. Willert, F. Scarano, C. J. Kähler, S. T. Wereley, and J. Kompenhans, *Particle image velocimetry: a practical guide*. Springer, 2018.

[31] L. A. Torres, B. A. Fleck, D. J. Wilson, and D. S. Nobes, "Calibration of a planar laser induced fluorescence technique for use in large scale water facilities," *Measurement*, vol. 46, no. 8, pp. 2597–2607, 2013.

[32] R. Jeppson, *Open channel flow: numerical methods and computer applications*. CRC Press, 2010.

[33] B. Fond, C. Abram, and F. Beyrau, "On the characterisation of tracer particles for thermographic particle image velocimetry," *Applied Physics B*, vol. 118, no. 3, pp. 393–399, 2015.

[34] I. Atthanayake, P. Denissenko, Y. Chung, and P. Thomas, "Formation–breakdown cycle of turbulent jets in a rotating fluid," *Journal of Fluid Mechanics*, vol. 868, pp. 666–697, 2019.

[35] W. Thielicke and E. Stamhuis, "Pivlab–towards user-friendly, affordable and accurate digital particle image velocimetry in matlab," *Journal of Open Research Software*, vol. 2, no. 1, 2014.

[36] L. Adrian, R. J. Adrian, and J. Westerweel, *Particle image velocimetry*. Cambridge University Press, 2011, no. 30.

[37] Z. Zhang, *LDA application methods: laser Doppler anemometry for fluid dynamics*. Springer Science & Business Media, 2010.

[38] H. Brunn, "Linearization and hot wire anemometry," *Journal of Physics E: Scientific Instruments*, vol. 4, no. 11, p. 815, 1971.

[39] C. G. Lomas, *Fundamentals of hot wire anemometry*. Cambridge University Press, 2011.

[40] Y. Takeda, *Ultrasonic Doppler velocity profiler for fluid flow*. Springer Science & Business Media, 2012, vol. 101.

[41] H. Bruun and H.-W. Anemometry, "Oxford science publications," *New York*, 1995.

[42] P. Sarathi, R. Gurka, G. A. Kopp, and P. J. Sullivan, "A calibration scheme for quantitative concentration measurements using simultaneous PIV and PLIF," *Experiments in Fluids*, vol. 52, no. 1, pp. 247–259, 2012.

[43] www.turnerdesigns.com, "Cyclops-7 submersible sensors," 2010.
[44] M. Pierobon and I. F. Akyildiz, "Diffusion-based noise analysis for molecular communication in nanonetworks," *IEEE Transactions on Signal Processing*, vol. 59, no. 6, pp. 2532–2547, 2011.
[45] A. Singhal, R. K. Mallik, and B. Lall, "Effect of molecular noise in diffusion-based molecular communication," *IEEE Wireless Communications Letters*, vol. 3, no. 5, pp. 489–492, Oct 2014.
[46] N. Farsad, W. Guo, C. Chae, and A. Eckford, "Stable distributions as noise models for molecular communication," in *IEEE Global Communications Conference (GLOBECOM)*, Dec 2015, pp. 1–6.
[47] X. Zeng, Y. Xia, and H. Tong, "Jackknife approach to the estimation of mutual information," *Proceedings of the National Academy of Sciences*, vol. 115, no. 40, pp. 9956–9961, 2018.
[48] G. Ritt, "Laser safety calculations for imaging sensors," *Sensors*, vol. 19, no. 17, p. 3765, 2019.